



## Effect of novel turbulators on the hydrothermal performance of counterflow double tube heat exchanger using nanofluids

Ebrahim Tavousi<sup>a</sup>, Noel Perera<sup>a,\*</sup>, Dominic Flynn<sup>b</sup>, Reaz Hasan<sup>a</sup>, Mostafizur Rahman<sup>a</sup>

<sup>a</sup> College of Engineering, Faculty of Computing, Engineering and the Built Environment, Birmingham City University, Birmingham, B4 7XG, UK

<sup>b</sup> Vehicle Efficiency, Jaguar Land Rover, Gaydon, CV35 0BJ, UK

### ARTICLE INFO

#### Keywords:

Double tube heat exchanger  
Turbulator insertion  
Nanofluid  
Nusselt number  
Heat transfer coefficient  
Pressure drop  
Thermal efficiency  
Rib

### ABSTRACT

Double pipe heat exchangers are widely used across various industries. Enhancing their performance not only benefits these industries but also contributes to reduced fossil fuel consumption and pollution. This study employs the passive method with a combination turbulator insertion and nanofluid technique to enhance the heat transfer rate and improve the double tube heat exchanger performance. The novelty of this study lies in the use of new turbulator insertions and various nanofluids to investigate the heat transfer and fluid flow characteristics under laminar and counter flow configuration. The study examined four types of turbulator insertions, including triangular, rectangular, trapezoidal, and oval, in conjunction with CuO, SiO<sub>2</sub>, Al<sub>2</sub>O<sub>3</sub> water-based nanofluids in a single-phase model. The findings revealed that the trapezoidal ribs exhibited higher Nusselt number and friction factor than the other rib shapes. Conversely, the oval ribs demonstrated a better performance evaluation criteria than the other rib shapes. Furthermore, the study explored different geometrical parameters such as rib width, height, and spacing, determining that rib height has the most significant impact on enhancing the heat transfer. The study achieved maximum performance evaluation criteria of 1.2 and 1.9 for SiO<sub>2</sub> nanofluid without turbulator insertion and with turbulator insertion, respectively.

### 1. Introduction

The demand for energy has been on the rise due to urbanization and the expanding global population. The use of gas, oil, coal, and other fossil fuels has adverse effects on the environment, contributing to the escalation of global warming. Therefore, adopting energy-saving measures and harnessing renewable energy sources represent effective solutions to mitigate this issue (Hosseinzadeh et al., 2020). One of the most commonly employed and crucial devices in both industrial and commercial settings is the double tube heat exchangers (DTHE). Therefore, creating an efficient thermal system within DTHERs can lead to cost reduction and substantial energy savings (Hussain and Sheremet, 2023; Venkatesh, 2023). DTHER represents the simplest form of a heat exchanger, wherein hot and cold fluids circulate in either parallel or counterflow configurations (Rao and Sankar, 2019). The utilization of DTHERs finds extensive application across various industries, including but not limited to chemical, food, oil, gas, pharmaceutical, solar energy, waste heat recovery, geothermal, combustion, latent heat energy storage, and air conditioning (Omidi et al., 2017; Li, 2022; Louis et al., 2022). Improving the heat transfer efficiency of heat exchangers

presents a notable challenge (Liu and Sakr, 2013; Rohsenow et al., 1998). Improving heat exchanger's performance can be categorized into three broad approaches: active, passive, and combined methods (Cancan et al., 2014). Active methods involve the application of external power to augment heat transfer through means such as vibration, electric fields, mechanical aids, or magnetic fields (Jadhav et al., 2016; Maleki et al., 2023). On the other hand, passive methods rely on extended surfaces and elements instead of external power (Hangi et al., 2022; Lalegani et al., 2018). Combined methods encompass the synergistic utilization of active and passive methods (Alam and Kim, 2018).

Tavousi, et al. (Tavousi et al., 2023) systematically classified passive methods into five main categories: turbulator insertion (Pourahmad and Pesteei, 2016), extended surface area (fins) (El Maakoul et al., 2020), geometry changes (Luo and Song, 2021), using nanofluids (Tavousi et al., 2023), and combinations of these techniques (Singh and Sarkar, 2021). A statistical investigation of more than 100 studies was conducted on the passive methods. The statistical investigation showed that the combined techniques of turbulator insertion and nanofluid have the maximum increase in heat transfer rate. A diverse range of turbulator insertions and nanofluids can be employed to enhance the performance

\* Corresponding author.

E-mail address: [noel.perera@bcu.ac.uk](mailto:noel.perera@bcu.ac.uk) (N. Perera).

<https://doi.org/10.1016/j.ijheatfluidflow.2024.109427>

Received 1 March 2024; Received in revised form 6 May 2024; Accepted 11 May 2024

Available online 17 May 2024

0142-727X/© 2024 The Authors. Published by Elsevier Inc. This is an open access article under the CC BY license (<http://creativecommons.org/licenses/by/4.0/>).

of DTHEs. Each combination of turbulator and nanofluid has a distinct impact on the heat transfer rate and the friction factor. For instance, the introduction of spiral springs, in the presence of  $\text{TiO}_2$  and  $\text{CuO}$  nanoparticles dispersed in water as nanofluids, demonstrated notable enhancements in the Nusselt number. Specifically, it led to a substantial increase of up to 117.39 % and 312 % for  $\text{TiO}_2$  and  $\text{CuO}$  nanofluids, respectively, in comparison to pure water without turbulator insertion (Gnanavel et al., 2020). The utilization of a cone-shaped insertion within a turbulent flow containing  $\text{Al}_2\text{O}_3$  and  $\text{CuO}$  nanofluids with a volume concentration of 1 % resulted in a remarkable augmentation of the Nusselt number and friction factor by 65 % and 50 %, respectively, for the  $\text{Al}_2\text{O}_3$  nanofluid (Karupphasamy et al., 2020). The employment of a tapered wire coil as a turbulator insertion with the hybrid nanofluid  $\text{Al}_2\text{O}_3$  and  $\text{MgO}$  under turbulent flow conditions with a volume fraction of 0.1 % yielded an enhancement up to 84 % in the Nusselt number and a 68 % increase in the friction factor (Singh and Sarkar, 2020).

Incorporating twisted tape insert and  $\text{Al}_2\text{O}_3$  nanofluid at 0.01 % and 0.03 % volume fractions resulted in a low increase in the Nusselt number and friction factor. The most notable enhancement observed was a 31.28 % increase in the Nusselt number, accompanied by a 23 % rise in the friction factor (Prasad and Gupta, 2016). The utilization of longitudinal strip inserts in conjunction with  $\text{Fe}_3\text{O}_4$  as a nanofluid under turbulent flow conditions yielded a maximum enhancement of 41.29 % in the Nusselt number, alongside a 36.7 % increase in the friction factor (Kumar et al., 2017). Furthermore, the integration of a rectangular rib turbulator in the presence of  $\text{Al}_2\text{O}_3$  nanofluid under laminar flow conditions demonstrated an increase in the Nusselt number by up to 50 %, ultimately resulting in the attainment of a maximum performance evaluation criteria (PEC) of 1.05 (Tavousi et al., 2023).

As Tavousi, et al. (Tavousi, et al., 2023) showed, the combination of turbulator insertion and nanofluid techniques has the greatest increase in heat transfer rate. However, limited studies have employed the

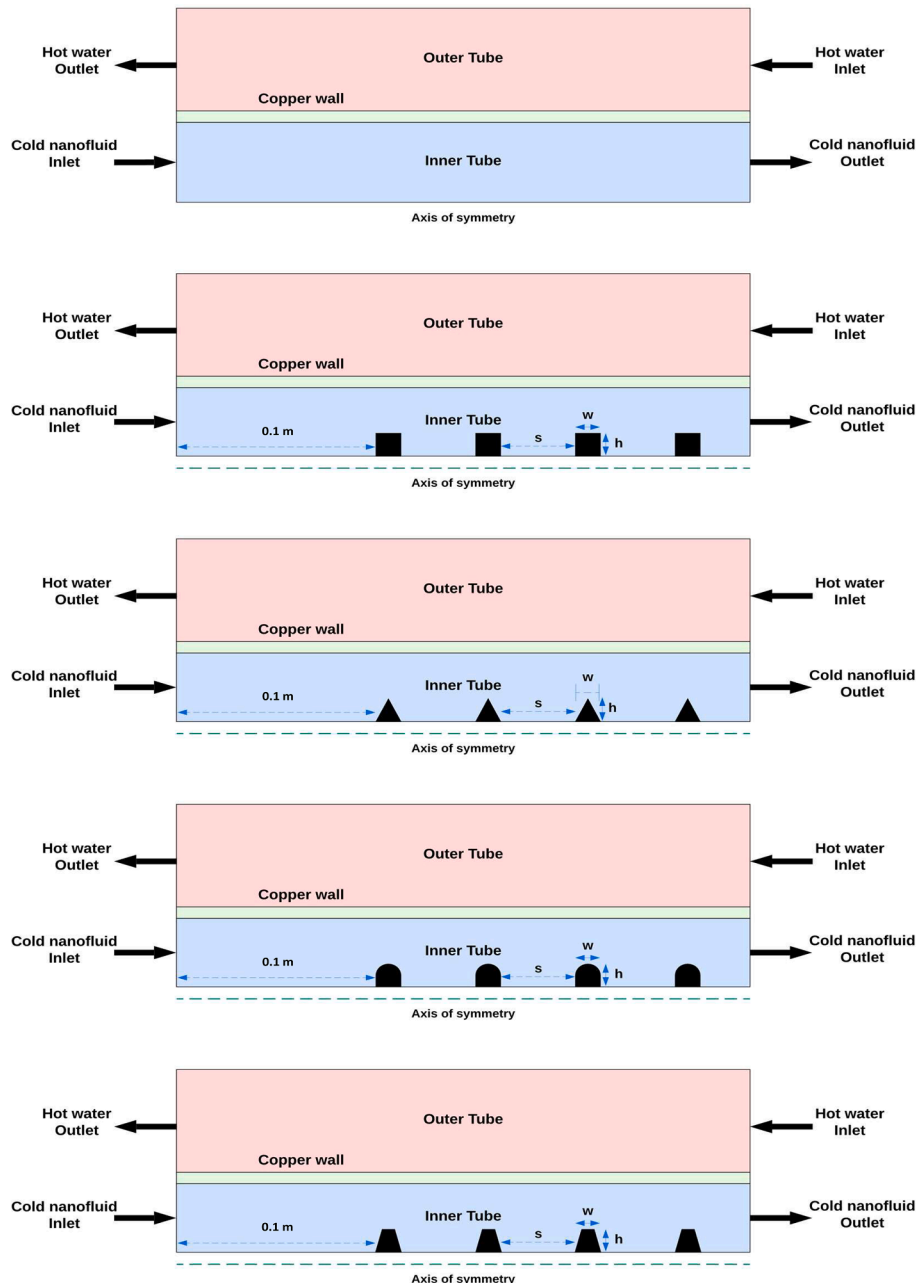


Fig. 1. Schematic of the analyzed DTHE, both with and without turbulator insertions.

insertion of turbulators in combination with nanofluids. This presents an opportunity for further augmentation of heat transfer rates in DTHEs. The current study follows this approach by incorporating newly designed turbulator inserts with distinct rib shapes (triangular, rectangular, trapezoidal, and oval) along with three different nanofluids: Al<sub>2</sub>O<sub>3</sub>, CuO, and SiO<sub>2</sub>. The primary objective of this study was to evaluate the effect of these rib shapes and nanofluids on heat transfer and fluid flow within a DTHE. Additionally, various aspect ratios of rib geometries were investigated to understand their influence on the laminar flow hydrothermal properties. The limitations of this study include the assumption of nanofluid homogeneity, the use of empirical correlations to determine nanofluid properties, and the omission of nanoparticle agglomeration and sedimentation effects.

## 2. Numerical setup

Fig. 1 illustrates the schematic of the analyzed DTHE, both with and without turbulator insertions. The inner tube has a diameter of 0.014 m, while the outer tube has a diameter of 0.08 m, with a total length of 1.8 m. Tube sizes (1/2 and 3 in.) were chosen based on their availability in the marketplace for practical and industrial relevance. The inner tube material is copper, with a thickness of 0.001 m. This study investigated four different turbulator insertions with varying rib shapes (triangular, rectangular, trapezoidal, and oval). Three key parameters were considered: the distances between the ribs (*s*), the height of the ribs (*h*), and the width of the ribs (*w*) as shown in Fig. 1. The turbulator insertion had a diameter of 0.002 m; in all cases, the first rib was located 0.01 m from the inlet of the DTHE. The flow within the DTHE is assumed to be axisymmetric along the longitudinal axis. The inner tube contains cold nanofluids with a constant inlet temperature of 295 K, while the outer tube is filled with pure hot water at a constant inlet temperature of 335 K. These temperatures were selected to align with common industrial practices to provide results that are more applicable to real-world scenarios (Eiamsa-ard et al., 2008; Lakew and Bolland, 2010; Padmanabhan et al., 2021). As some published work concluded that the single-phase approach and constant thermophysical properties of fluids agree with the experimental results, these two approaches were selected for the numerical investigation (Eshgarf et al., 2023; Albojamal and Vafai, 2017). The assumption of constant thermophysical properties of nanofluid was considered in this study. The results of the constant thermophysical properties compared to dependent thermophysical properties showed less than 2 % deviation. Laminar flow conditions were considered for the inner and outer tubes, with a Reynolds number of 800 maintained for the outer tube and a range of Reynolds numbers between 400 and 2000, in increments of 400, for the inner tube. The working fluid in the inner tube consisted of three nanofluids, CuO, SiO<sub>2</sub>, and Al<sub>2</sub>O<sub>3</sub> each with a volume fraction of 0.05. Detailed thermophysical properties of the used materials in this study are provided in Table 1.

## 3. Governing equations

This research investigates the heat transfer properties and fluid dynamics of laminar flow in a DTHE. The governing equations for solving flows in the DTHE, including continuity, momentum and energy for laminar flow in steady states, are as follows (Iwaniszyn, 2021).

In the case of steady and incompressible flow, the continuity equation is expressed as follows:

tion is expressed as follows:

$$\frac{\partial u}{\partial x} + \frac{\partial v}{\partial y} + \frac{\partial w}{\partial z} = 0 \quad (1)$$

For incompressible flow with constant viscosity, the momentum equation can be expressed as follows:

$$\nabla \cdot (\rho \mathbf{V}\mathbf{V}) = -\nabla P + \nabla \cdot (\mu \nabla \mathbf{V}) \quad (2)$$

For incompressible flow where the thermal conductivity remains constant, the energy conservation equation can be expressed as follows:

$$\nabla \cdot (\rho \mathbf{V}C_p T) = \nabla \cdot (k \nabla T) \quad (3)$$

Where  $\rho$ ,  $C_p$ , and  $k$  represent density, specific heat, and thermal conductivity, respectively.

Present study employed Al<sub>2</sub>O<sub>3</sub>, CuO, and SiO<sub>2</sub> water-based nanofluids as incompressible working fluids with constant thermophysical properties. These nanofluids' density and specific heat capacity are determined based on the nanoparticle volume fraction (Akbari et al., 2017; Kamyar et al., 2012; Bergman, 2009). The thermal conductivity and viscosity of the nanofluids are calculated using equations proposed by Vajjha (Vajjha and Das, 2009) and Sharma (Sharma et al., 2012), respectively. Notably, in these equations, thermal conductivity and viscosity depend on temperature, nanoparticle size, and volume fraction. These considerations lead to the results being closely aligned with experimental data. The properties of the nanofluids were derived from the following equations.

$$\rho_{nf} = (1 - \varphi)\rho_b + \varphi\rho_p \quad (4)$$

$$(C_p)_{nf} = (1 - \varphi)(C_p)_b + \varphi(C_p)_p \quad (5)$$

$$\frac{\mu_{nf}}{\mu_b} = \left(1 + \frac{\varphi}{100}\right)^{11.3} \times \left(1 + \frac{T_{nf}}{70}\right)^{-0.038} \times \left(1 + \frac{d_p}{170}\right)^{-0.061} \quad (6)$$

$$\frac{k_{nf}}{k_b} = \left[ \frac{k_p + 2k_b - 2(k_b - k_p)\varphi}{k_p + 2k_b + (k_b - k_p)\varphi} \right] \times 5 \times 10^4 \beta \varphi \rho_b C_{p,b} \sqrt{\frac{\kappa T}{\rho_p d_p}} f(T, \varphi) \quad (7)$$

$$f(T, \varphi) = (2.8217 \times 10^{-2} \varphi + 3.917 \times 10^{-3}) \left(\frac{T}{T_0}\right) + (-3.0669 \times 10^{-2} \varphi - 3.91123 \times 10^{-3}) \quad (8)$$

The subscripts p, nf, and b denote particles, nanofluid, and base fluid, respectively.

The equations below can be used to determine the overall convection heat transfer coefficients, as well as the Nusselt number for nanofluids flowing inside a tube with an inner radius of  $R_{in}$  (Lin et al., 2022; Ahmed et al., 2016).

$$\overline{h}_{nf} = \frac{1}{L} \int_0^L h_{nf} \cdot dx_{r=R_{in}} \quad (9)$$

$$\overline{Nu}_{nf} = \frac{\overline{h}_{nf} (2R_{in})}{k_{in}} \quad (10)$$

Table 1

Thermophysical properties of used materials at 300 K and 40 nm for nanoparticles in this research.

| Thermophysical properties   | Water (Incropera et al., 1996) | Al <sub>2</sub> O <sub>3</sub> (Mohammed et al., 2013) | CuO (Mohammed et al., 2013) | SiO <sub>2</sub> (Mohammed et al., 2013) | Copper (Tian et al., 2020) |
|-----------------------------|--------------------------------|--|-----------------------------|--|----------------------------|
| $\rho$ (kg/m <sup>3</sup> ) | 997                            | 3600   | 6500                        | 2200                                     | 8978                       |
| $C_p$ (J/kg K)              | 4179                           | 765  | 535.6                       | 703                                      | 381                        |
| $k$ (W/m K)                 | 0.613                          | 36   | 20                          | 1.2                                      | 387.6                      |
| $\mu$ (N s/m <sup>2</sup> ) | 0.000855                       | –  | –                           | –  | –                          |

The subscript b denotes a bulk or average value, while L represents the length of the tube.

The Nusselt number's empirical relationship for both inner and outer tubes in laminar flow conditions is described as follows (Sieder and Tate, 1936):

$$Nu = 1.86 \left( RePr \frac{d}{L} \right)^{0.33} \quad (11)$$

Where  $Re$  stands for the Reynolds number,  $Pr$  represents the Prandtl number,  $d$  is the tube diameter, and  $L$  denotes the length of DTHE.

The pressure drop along a tube of length  $L$  can be determined using the following equation (White, 1979).

$$\Delta P = \frac{fL\rho V^2}{2d_h} \quad (12)$$

Where  $f$ ,  $L$ ,  $\rho$ , and  $d_h$  are the friction factor, length of DTHE, density the hydraulic diameter of the tube cross-section, respectively.

The PEC (thermal efficiency) of DTHE can be obtained from the following equation (Noorbakhsh et al., 2022).

$$PEC = \frac{\left( \frac{Nu}{Nu_0} \right)}{\left( \frac{f}{f_0} \right)^{1/3}} \quad (13)$$

Where the subscript 0 indicates the base fluid without nanoparticles.

The relative error  $e_r$  can be calculated as follows.

$$e_r = \frac{|\varepsilon - \hat{\varepsilon}|}{\hat{\varepsilon}} \times 100 \quad (14)$$

In which  $\varepsilon$  represents the target parameter, and  $\hat{\varepsilon}$  represents the corresponding target parameter in the highest mesh element numbers.

To define the dimensionless key parameters for  $s$ ,  $w$ , and  $h$ , the following expressions were used.

$$S = \frac{s}{R_i} \quad (15)$$

Where  $R_i$  is the radius of the inner tube.

## 4. Data production

### 4.1. Numerical method

Ansys Workbench 2022 was used to simulate the governing equations. The finite volume method was employed to discretize the governing equations under laminar forced convection, including continuity, momentum, and energy. A coupled approach was established for the velocity–pressure interactions, and a second-order upwind scheme was employed to solve the momentum and energy equations. For the convergence of numerical calculation, the residuals were set at  $10^{-6}$  for all variables. The values of the three dimensionless key parameters ( $S$ ,  $W$ , and  $H$ ), as derived from Equation (15), with the selected dimensions for  $s$ ,  $w$ , and  $h$ , are presented in Table 2.

**Table 2**  
The value of dimensionless key parameters.

| $s$ [m] | $S$   | $w$ [m] | $W$  | $h$ [m] | $H$  |
|---------|-------|---------|------|---------|------|
| 0.02    | 2.86  | 0.001   | 0.14 | 0.001   | 0.14 |
| 0.04    | 5.71  | 0.002   | 0.29 | 0.002   | 0.29 |
| 0.06    | 8.57  | 0.003   | 0.43 | 0.003   | 0.43 |
| 0.08    | 11.43 | 0.004   | 0.57 | 0.004   | 0.57 |
| 0.10    | 14.29 | 0.005   | 0.71 | 0.005   | 0.71 |

### 4.2. Grid independence

The influence of varying mesh densities on heat transfer and hydrodynamic parameters was examined to ensure the adequacy of mesh refinement and independence in the computational simulations. Three parameters were considered to check the mesh independence test, including outlet temperature, pressure drop, and average Nusselt number of the inner tube. Fig. 2. shows that the optimal mesh is approximately 107 k elements and that the maximum error compared to the highest mesh density was less than 2.2%. Also, it was concluded that the Nusselt number was more sensitive to the number of elements compared to the other parameters. Fig. 3. displays a structured mesh of the rectangular rib featuring a finer mesh closer to the wall and the turbulator. The boundary conditions were defined as follows: velocity inlets for the inlets of both inner and outer tubes, pressure outlets for the outlets of both inner and outer tubes, no-slip conditions for the tube walls, and adiabatic for the outer wall of the outer tube.

### 4.3. Validation

In order to validate the results obtained from numerical simulations, a comparison was undertaken with both experimental data and the results of the simulation derived from the two-phase approach simulation. Fig. 4. displays the average Nusselt number results against Reynolds number obtained using the empirical correlations presented by Seider and Tate (Sieder and Tate, 1936) (eq. (11), Shah and London (Shah and London, 2014), Gnielinski (Gnielinski, 1976), and Hausen (Hausen, 1959) for laminar flow with pure water. In this case, the inlet temperatures for the inner and outer tubes were set at 280 K and 350 K, respectively. The Reynolds number for the outer tube was held constant at 800. The results of present study revealed a maximum deviation of 5.64% when compared to the findings reported by Seider and Tate (Sieder and Tate, 1936) results. Additionally, another validation was carried out for the  $Al_2O_3$  nanofluid, aiming to compare the results of the average Nusselt number ratio for the inner tube with numerical data from the two-phase model conducted by Shirvan, et al. (Shirvan et al., 2017) and experimental data from Heyhat, et al. (Heyhat et al., 2013). The DTHE dimensions used in this case were 0.005 m diameter for the copper inner tube with a thickness of 0.0005 m and a length of 2 m. The outer tube was utilized as a steam bath to maintain a constant temperature within the system, and the inlet temperature was 333.15 K for the inner tube. Fig. 5. illustrates the validation results of the ratio of the average Nusselt number for the nanofluid compared to pure water against various Reynolds numbers. The maximum deviation observed in the current study with the single-phase model, compared to the experimental results, was less than 5.42%, while the maximum deviation of

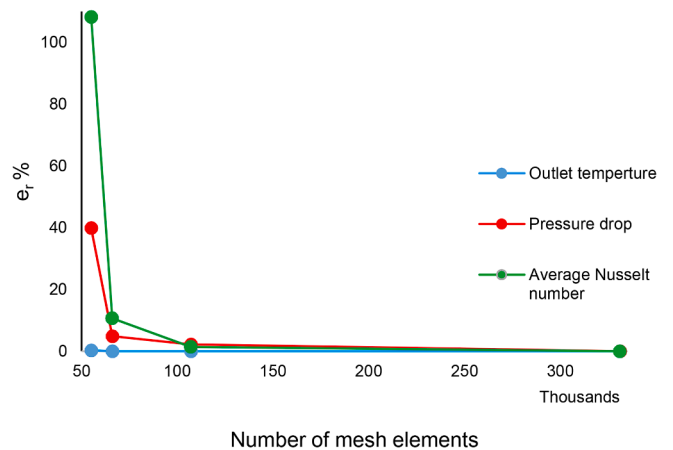


**Fig. 2.** Relative error of the selected parameters for different number of mesh elements.

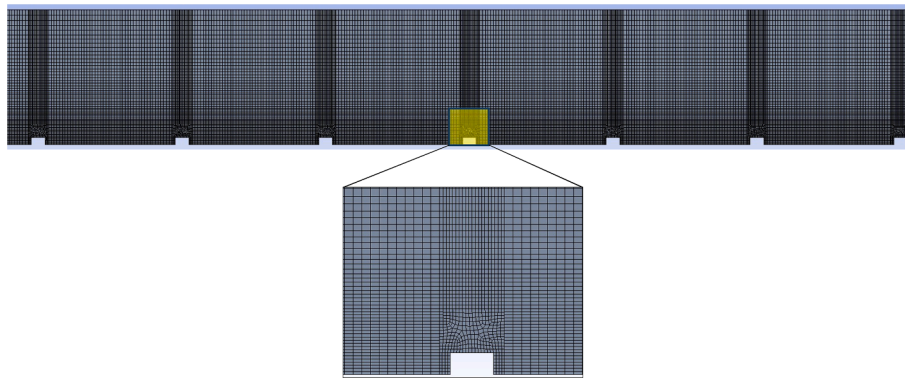


Fig. 3. The structured mesh of rectangular ribs.

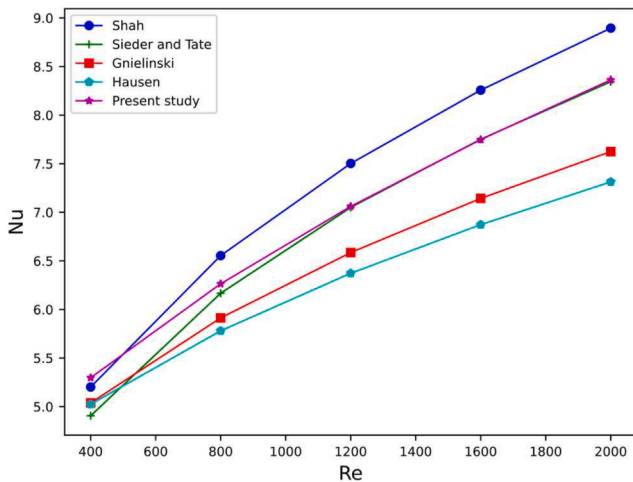


Fig. 4. Results of the present study vs empirical correlations results for average Nusselt number in counter flow using pure water.

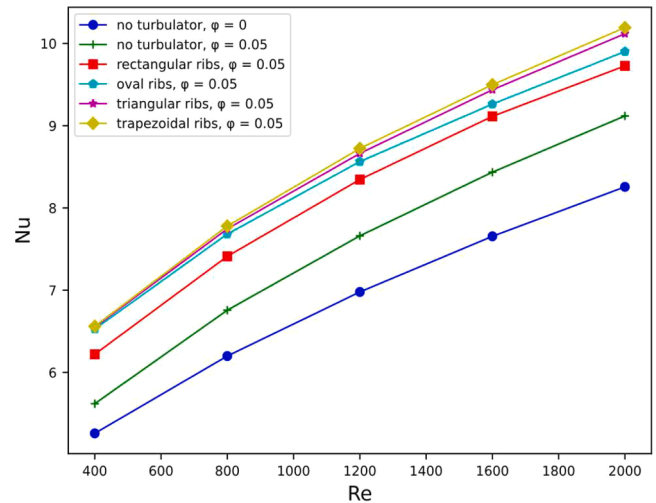


Fig. 6. The average Nusselt number against Reynolds numbers for various rib shapes, CuO nanofluid  $\phi = 0.05$ ,  $S = 5.71$ ,  $W = 0.29$ , and  $H = 0.29$ .

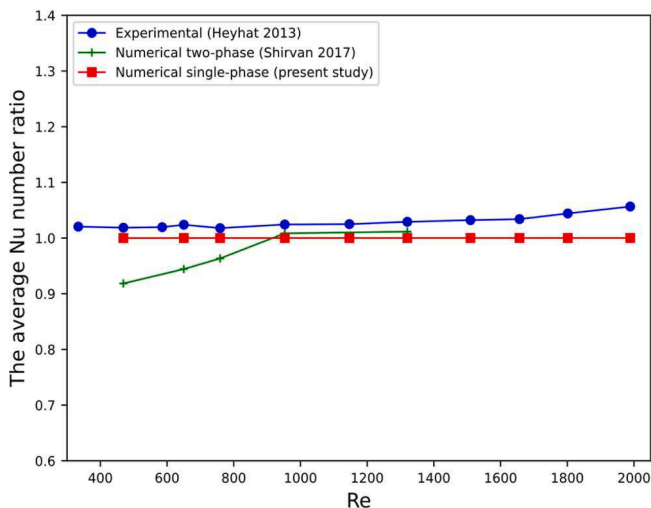


Fig. 5. Results of present study with numerical two-phase model and experimental results for  $Al_2O_3$  nanofluid at  $\phi = 0.01$ .

the two-phase model was less than 9.83 %.

### 5. Results and discussion

Fig. 6 illustrates the average nusselt number of the inner tube against

reynolds numbers for various rib shapes and cuo nanofluid. the data indicates that the utilization of nanofluid leads to a notable increase in the nusselt number compared to using pure water, and this effect is further enhanced when turbulator insertion is employed. specifically, the trapezoidal and triangular turbulators exhibit the higher nusselt numbers, with trapezoidal ribs yielding the superior results compared to other rib shapes. On the other hand, the rectangular ribs showed the least increase in Nusselt number among all the different rib shapes. The observed rise in the Nusselt number can be attributed to two main factors. Firstly, the incorporation of nanoparticles enhances the thermal properties of the working fluid. Secondly, the insertion of turbulator induces additional mixing and secondary flow, which reduces the thermal boundary layer close to the wall. The Nusselt number increases with the increase of the Reynolds number due to an increase in momentum and mixing flow. These combined effects of nanoparticles and turbulator insertion lead to improved heat transfer performance of the DTHE.

Fig. 7 depicts the inner tube's pressure drop and friction factor-against Reynolds numbers for various rib shapes and CuO nanofluid. The addition of nanoparticles to the working fluid increases the pressure drop compared to pure water, and this increase becomes more pronounced when a turbulator is inserted into the DTHE. The pressure drop and friction factor are critical parameters that affect the performance of DTHEs. The figures reveal that the triangular rib shape exhibits the highest pressure drop and friction factor, whereas the oval turbulator demonstrates the lowest values. The triangular rib shape, by virtue of its shape, is likely to present a more abrupt obstruction to the flow, leading

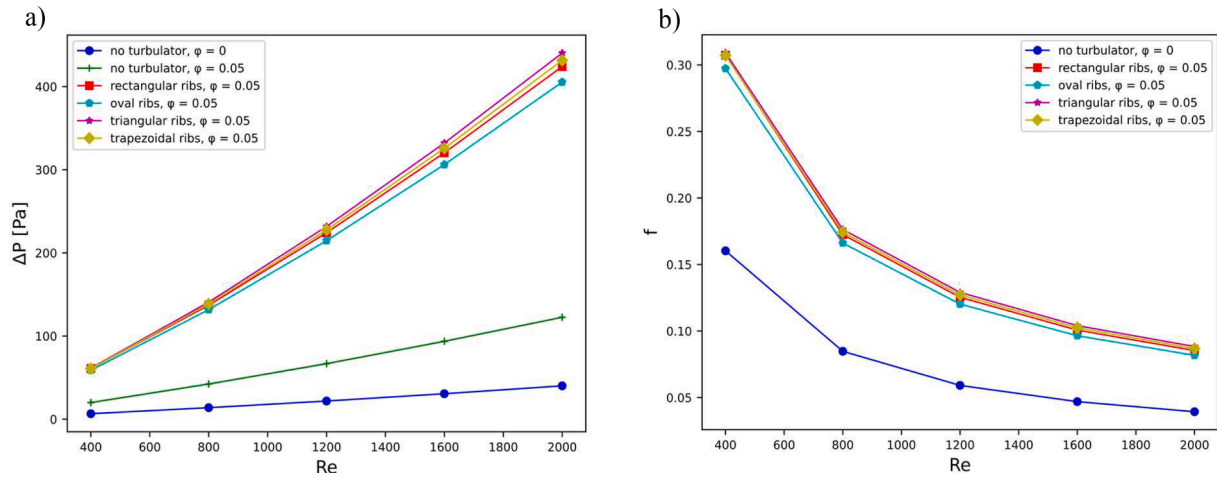


Fig. 7. A) the pressure drop and b) friction factor against Reynolds numbers for various rib shapes, CuO nanofluid  $\phi = 0.05$ ,  $S = 5.71$ ,  $W = 0.29$ , and  $H = 0.29$ .

to increased flow separation and consequently higher energy losses. This phenomenon is further compounded by the formation of a more pronounced recirculation zone behind the rib, which contributes to an increase in the system's overall resistance to flow, reflected in the heightened pressure drop. Comparatively, the trapezoidal rib, while still inducing a significant pressure drop, might offer a slightly less aggressive interruption to the flow due to their sloped faces. The gradient provided by the trapezoidal shape potentially allows for a more gradual deviation of the flow, which in turn might result in a somewhat reduced pressure drop relative to triangular ribs. Due to its longer length at the top of the shape, the rectangular rib induces a lower pressure drop. Conversely, the oval rib, characterized by a smoother surface, diminishes the friction between the flow and the turbulator. This results in a reduced pressure drop and friction factor compared to other shapes.

Fig. 8 illustrates the recirculation lengths associated with different rib geometries in a flow with a Reynolds number of 1200, using CuO nanofluid at a volume fraction  $\phi = 0.05$ . The recirculation zones, a key factor in the enhancement of heat transfer, are initiated at the flow separation points, locations proximate to the top of the ribs, and extend downstream to the points of flow reattachment on the turbulator wall. In a descending order of length, the trapezoidal rib induces the longest recirculation zone, followed by the triangular rib, then the oval, and finally the rectangular rib, which generates the shortest length. The length of the recirculation zone is crucial, as it directly influences the intensity of fluid mixing and the generation of secondary flow patterns within the flow field. The secondary flow is instrumental in disrupting thermal boundary layers and augmenting convective heat transfer, as quantified by the Nusselt number. Hence, the data imply that the ribs with trapezoidal and triangular shapes are more effective in enhancing the heat transfer rate compared to those with oval and rectangular shapes. This phenomenon is attributable to the more pronounced fluid dynamic activities within the recirculation zones created by the

trapezoidal and triangular rib configurations.

Fig. 9 presents the average Nusselt number of the inner tube plotted against Reynolds numbers for different ratios of the height of the trapezoidal rib to the radius of the inner tube ( $h$ ) in the presence of SiO<sub>2</sub> nanofluid. The graph demonstrates that as the  $H$  increases, the Nusselt number shows an upward trend. This phenomenon can be attributed to the enhanced mixing and secondary flow resulting from the increased obstruction in the flow caused by the trapezoidal rib. As a result, the thermal boundary layer decreases, leading to an overall increase in heat

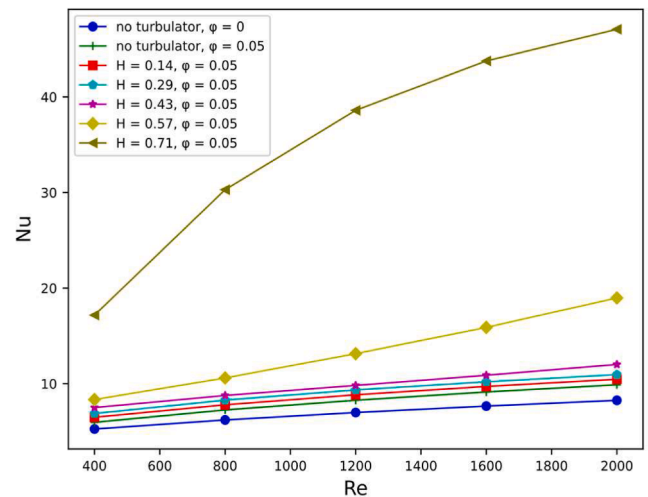


Fig. 9. The average Nusselt number and heat transfer coefficient of inner tube against Reynolds numbers for different  $H$ , SiO<sub>2</sub> nanofluid  $\phi = 0.05$ ,  $S = 5.71$ , and  $W = 0.29$ .

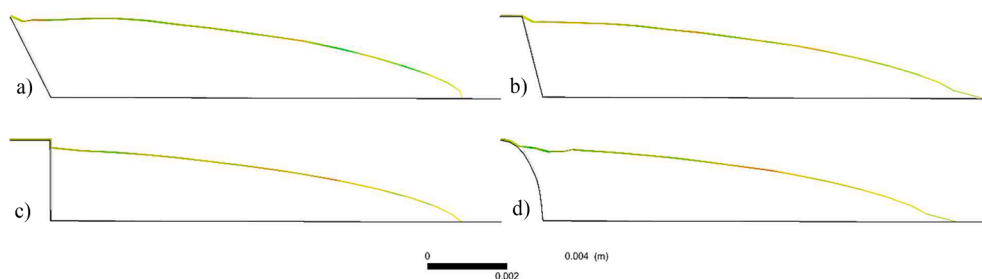


Fig. 8. Recirculation length of a) triangular, b) trapezoidal, c) rectangular, and d) oval ribs for Reynolds number of 1200, CuO nanofluid  $\phi = 0.05$ ,  $S = 5.71$ ,  $W = 0.29$ , and  $H = 0.29$ .

transfer. Furthermore, a noticeable enhancement occurs at  $H = 0.57$ , where the average Nusselt number of the DTHE exceeds 40. These results indicate a significant improvement in the average Nusselt number at this specific  $H$  value compared to the other  $H$  values. The Nusselt number of all cases shows an increasing trend with the rise in the Reynolds number.

Fig. 10 the inner tube's pressure drop and friction factor are depicted against Reynolds numbers for different ratios of the height of the trapezoidal rib to the radius of the inner tube ( $h$ ) in the presence of  $\text{SiO}_2$  nanofluid. The graph clearly illustrates that both the pressure drop and friction factor increase as the value of  $H$  increases. This is attributed to the greater obstruction in the flow resulting from the increased rib height. Notably, the impact of this increase is significant for  $H = 0.71$ , where the flow experiences maximum obstruction.

Figs. 11 and 12. present the inner tube's average Nusselt number, pressure drop, and friction factor against Reynolds numbers. These figures illustrate the impact of rectangular ribs and varying ratios of the distances between the ribs to the inner tube radius ( $S$ ) when  $\text{Al}_2\text{O}_3$  nanofluid is used. The findings indicate a significant improvement in the average Nusselt number, pressure drop, and friction factor when a turbulator is utilized, compared to where no turbulator is employed or when nanofluid is used alone. When the distances between ribs exceed a value of  $S = 5.71$ , there is only a minor influence on the average Nusselt number, pressure drop, and friction factor. However, as the distances between the ribs decrease, the number of ribs increases, leading to interactions between the flow and the rib obstacles at closer distances. Consequently, this generates enhanced secondary flow and increased mixing within the fluid stream. Furthermore, it can be deduced that the parameter  $S$  exerts a greater effect on the heat transfer and fluid flow characteristics than the parameter  $W$ . However, its effect is less significant than parameter  $H$ .

Figs. 13 and 14. represent the average Nusselt number, pressure drop, and friction factor of the inner tube against Reynolds numbers for different ratios of the rectangular rib width to the inner tube radius ( $W$ ) in the presence of  $\text{SiO}_2$  nanofluid. The findings reveal a substantial enhancement in the average Nusselt number, pressure drop, and friction factor when employing a turbulator and nanofluid compared to cases with no turbulator and nanofluid alone. These figures demonstrate that changes in the parameter  $W$  have a limited impact on the average Nusselt number, pressure drop, and friction factor. For example, the change in the average Nusselt number for  $\text{Re} = 1200$  between values of  $W = 0.43$  and  $0.57$  is  $0.26\%$ . However, the corresponding percentage changes for  $\text{Re} = 1200$  for  $S = 8.57$  and  $5.71$  and  $H = 0.43$  and  $0.57$  are observed to be  $2.36\%$  and  $33.85\%$ , respectively. So, variations in  $W$  exhibit a minimal influence on generating secondary flow and mixing

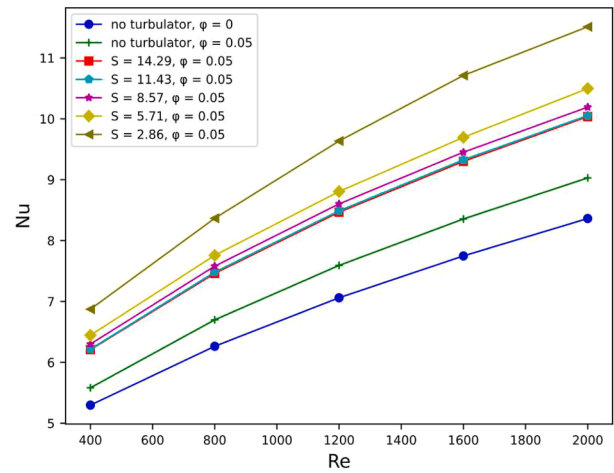


Fig. 11. The average Nusselt number of inner tube against Reynolds numbers for different  $S$ ,  $\text{Al}_2\text{O}_3$  nanofluid  $\phi = 0.05$ ,  $W = 0.29$ , and  $H = 0.29$ .

within the fluid stream. For all cases, it is observed that the average Nusselt number and pressure drop increased with an increase in Reynolds number, while the friction factor decreases with increasing Reynolds number.

Fig. 15 presents colour plots illustrating the a) normalized temperature, b) normalized velocity magnitude, c) normalized radial velocity, and d) pressure coefficient for various shapes, including triangular, trapezoidal, rectangular, and oval, using the  $\text{CuO}$  nanofluid with a  $\phi = 0.05$ . The results show that the trapezoidal, triangular, and oval shapes exhibit a more uniform normalized temperature distribution than the rectangular shape. This suggests that the mixing and secondary flow contribute to a more evenly distributed temperature in the flow. Furthermore, the triangular shape experiences the highest intensity of pressure coefficient, while the oval shape exhibits the lowest. This phenomenon is attributed to the creation of smoother obstacles in the path of the flow, leading to variations in pressure distribution. The normalized velocity magnitude and normalized radial velocity plots provide insights into the flow patterns around the different shapes and describe the formation of vortices behind each rib. It can be seen that the change in normalized magnitude velocity and normalized radial velocity is more pronounced in triangular and trapezoidal shapes when compared to rectangular and oval shapes.

Fig. 16 presents color plots that visually represent the a) normalized temperature and b) normalized velocity magnitude at various heights of trapezoidal ribs using a  $\text{SiO}_2$  nanofluid with  $\phi = 0.05$ . The findings

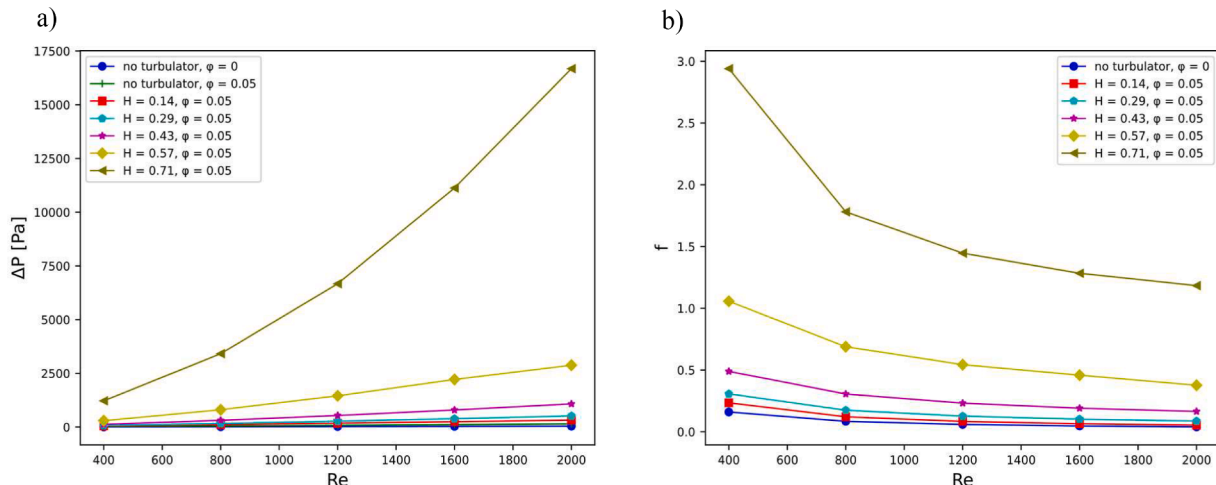


Fig. 10. A) the pressure drop and b) friction factor of inner tube against Reynolds numbers for different  $h$ ,  $\text{SiO}_2$  nanofluid  $\phi = 0.05$ ,  $S = 5.71$ , and  $W = 0.29$ .

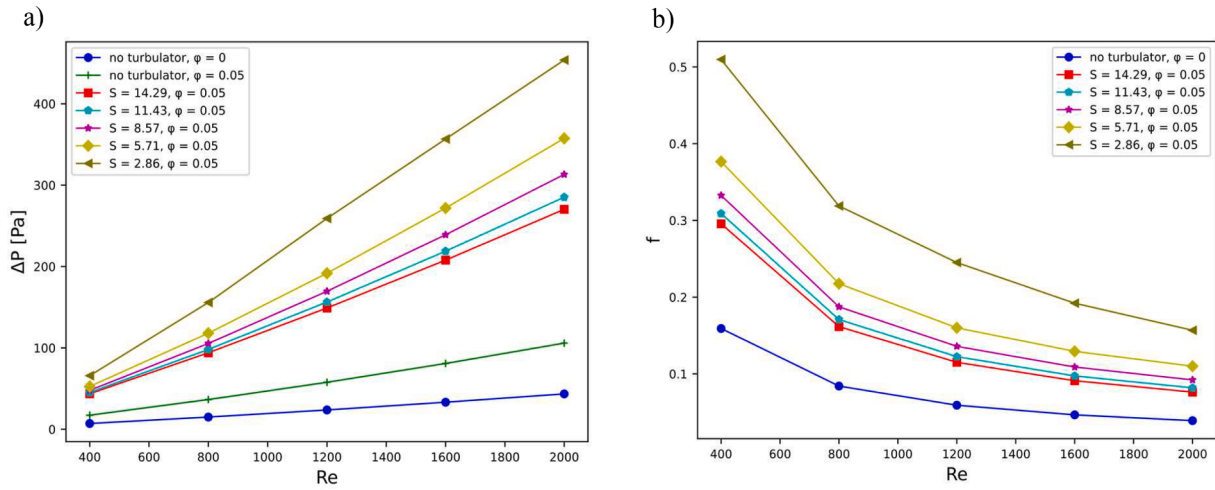


Fig. 12. A) the pressure drop and b) friction factor of inner tube against Reynolds numbers for different  $s$ ,  $Al_2O_3$  nanofluid  $\phi = 0.05$ ,  $W = 0.29$ , and  $H = 0.29$ .

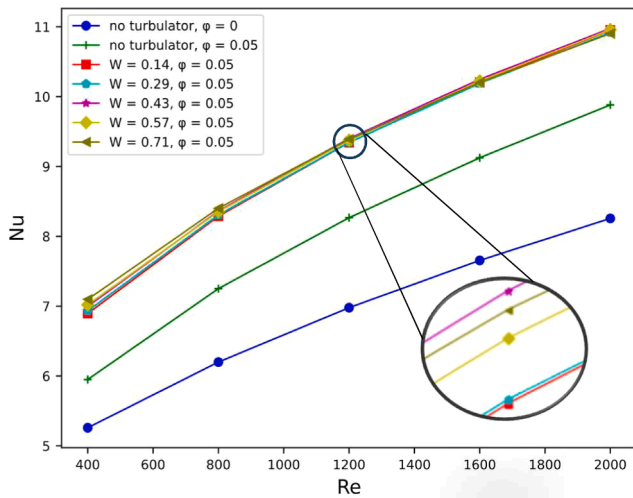


Fig. 13. The average Nusselt number of inner tube against Reynolds numbers for different  $W$ ,  $SiO_2$  nanofluid  $\phi = 0.05$ ,  $S = 5.71$ , and  $H = 0.29$ .

indicate that when the height of the ribs is increased, the temperature distribution within the flow becomes more uniform. This uniformity is attributed to enhanced mixing and the development of secondary flow

patterns caused by the presence of taller obstacles in the flow path. As a result of these effects, the thermal boundary layer is disrupted after passing each rib, reducing its thickness. This reduction contributes to an improved heat transfer rate within the system. However, as the height of the ribs increases, the velocity magnitude reveals the formation of vortices and a corresponding decrease in flow velocity. This phenomenon results in an increase in pressure drop across the system.

Fig. 17 illustrates the percentage enhancement of a) the average nusselt number and b) pressure drop of the three nanofluids without turbulator insertion and with  $re = 2000$  and a volume fraction  $\phi = 0.05$ , compared to water and without turbulator insertion. The findings indicated that the  $SiO_2$  nanofluid exhibits the highest Nusselt number and pressure drop rise when compared to  $CuO$  and  $Al_2O_3$  nanofluids. This difference can be attributed to  $SiO_2$ 's lower thermal conductivity and density compared to the other nanoparticles. As a result, at the same Reynolds number,  $SiO_2$  achieves a higher average velocity. This increased fluid velocity significantly impacts the heat transfer coefficient and forced convection.

Fig 18 illustrates the ratio of the average nusselt number and friction factor for  $SiO_2$  and various dimensionless parameters,  $W$ ,  $S$ , and  $H$ , to the average Nusselt number and friction factor of water without turbulator insertion. This figure indicates that the height of the ribs exerts the most significant influence on enhancing the heat transfer rate while also resulting in the highest friction factor. Conversely, the width of the ribs has the least impact on both heat transfer rate and friction factor. This

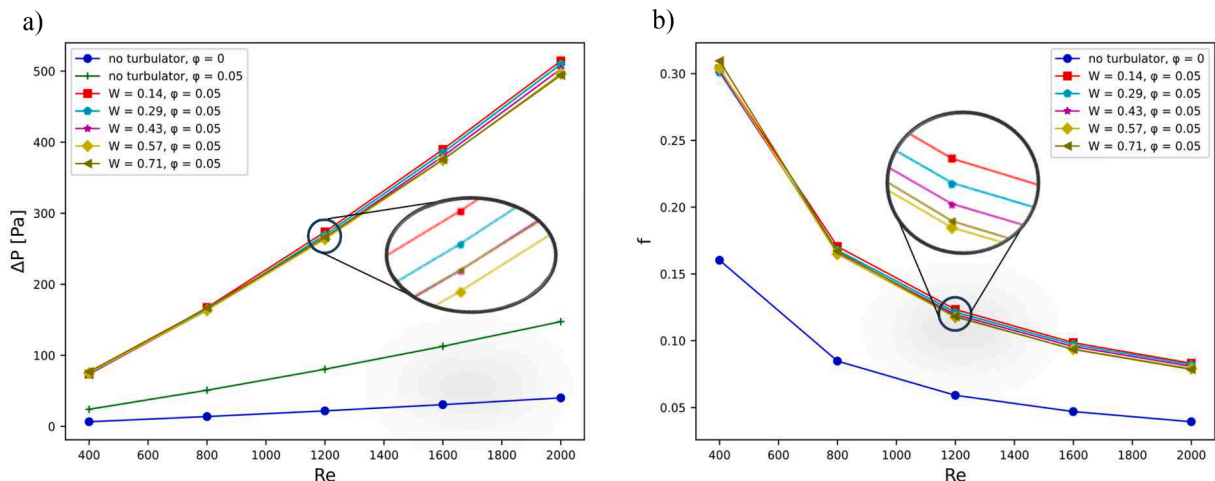


Fig. 14. A) the pressure drop and b) friction factor of inner tube against Reynolds numbers for different  $w$ ,  $SiO_2$  nanofluid  $\phi = 0.05$ ,  $S = 5.71$ , and  $H = 0.29$ .

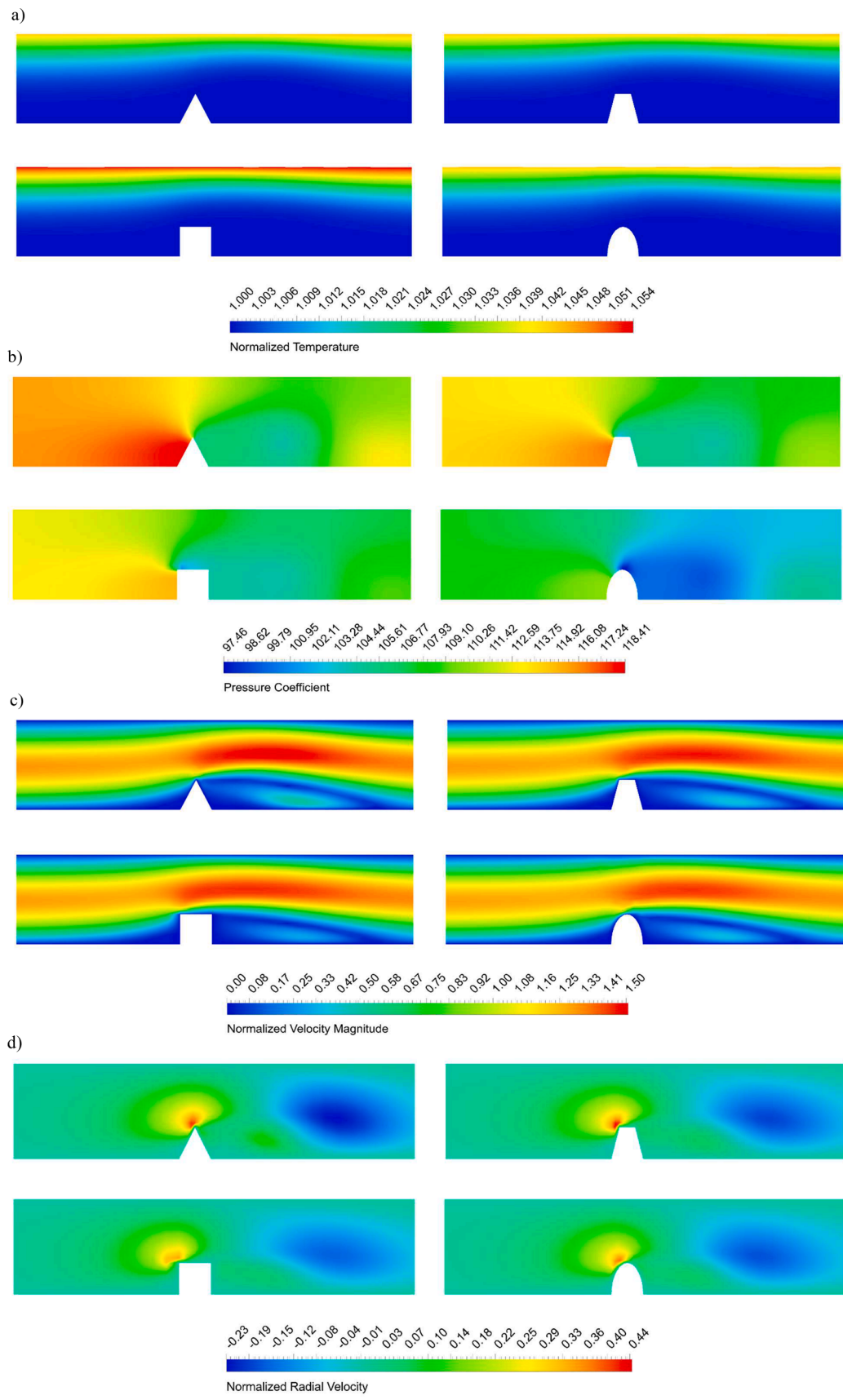
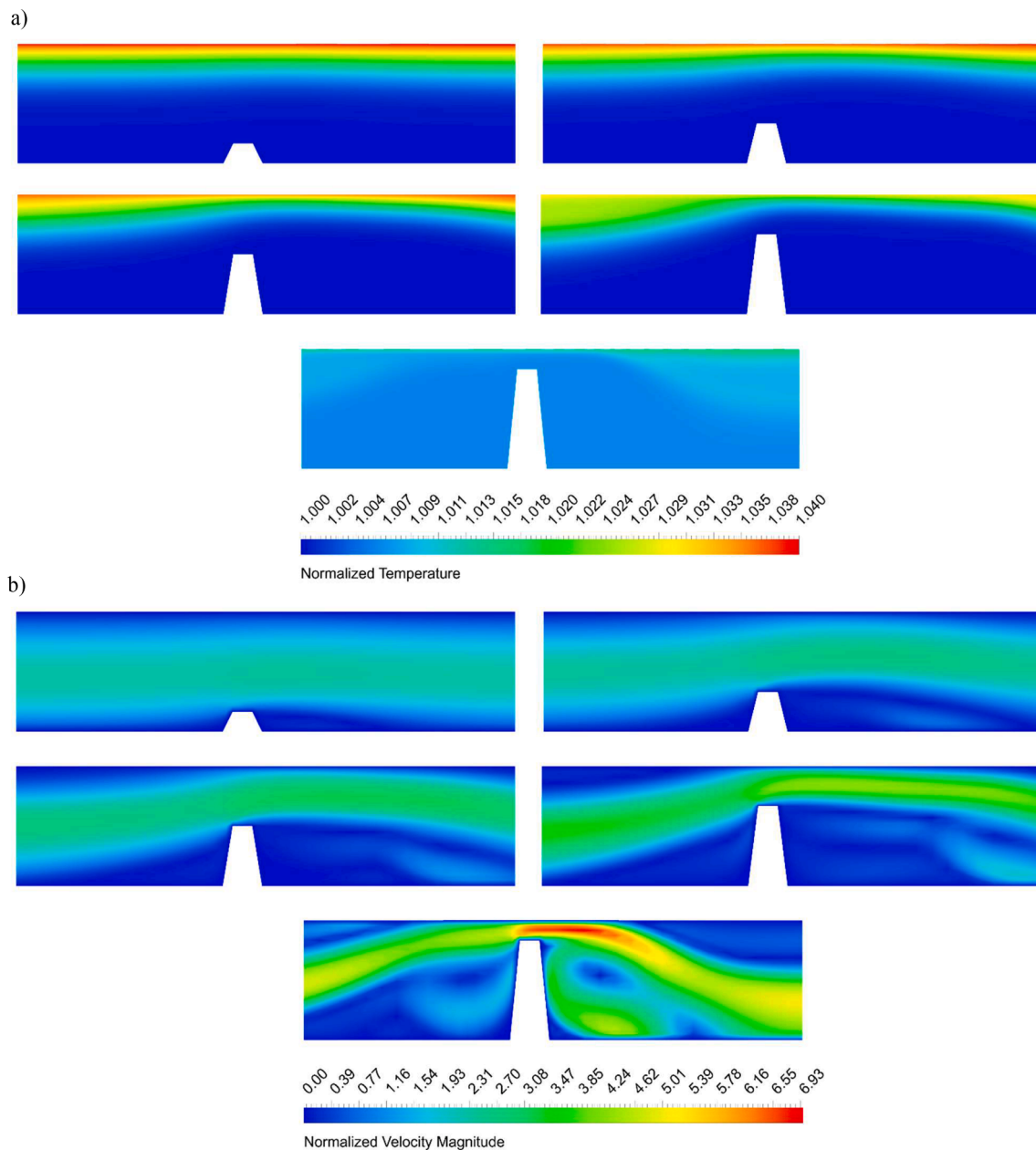


Fig. 15. Colour plots of a) normalized temperature, b) pressure coefficient, c) normalized velocity magnitude, and d) normalized radial velocity for different geometries, utilizing CuO nanofluid at  $Re = 800$ ,  $\phi = 0.05$ ,  $S = 5.71$ ,  $W = 0.29$ , and  $H = 0.29$ .



**Fig. 16.** Colour plots of a) normalized temperature and b) normalized velocity magnitude for different height, utilizing  $\text{SiO}_2$  nanofluid at  $\text{Re} = 1200$ ,  $\phi = 0.05$ ,  $S = 5.71$ , and  $W = 0.29$ .

occurs because taller ribs induce more mixing and secondary flow, which reduces the thermal boundary layer. The spacing between the ribs ranks as the second most influential parameter. Decreasing the distance between the ribs increases the number of ribs, leading to higher heat transfer rates and friction factors. The comparative analysis of the results, emphasizing the increased heat transfer, alongside the statistical investigation by Tavousi, et al. (Tavousi et al., 2023) (Fig. 19.) regarding enhanced heat transfer through the combination turbulator insertion and nanofluid techniques, indicates that the improvement in heat transfer rate observed in the current study exceeds the average outcomes previously reported. In their study, the average heat transfer rate enhancement was approximately 125%, while the maximum increase of the average Nusselt number reached about 470%.

Fig. 20 shows the PEC for different shapes of ribs and Fig. 21. shows the maximum PEC for all cases studied including using nanofluid alone with no turbulator and using turbulator insertion and  $\text{SiO}_2$  nanofluid. PEC is a significant parameter that relates the useful criteria (Nusselt

number) to the penalty criteria (friction factor) and provides valuable insights into the performance of heat exchangers. It can be observed that the trapezoidal turbulator exhibits the highest Nusselt number and heat transfer coefficient. However, the oval turbulator shows the highest PEC due to its lower friction factor when compared to the other turbulator shapes. The rectangular turbulator had the worst PEC, as it exhibited the lowest improvement in Nusselt number and heat transfer coefficient while having a high friction factor. The triangular ribs had the highest friction factor among the four turbulators, resulting in a low PEC. It was concluded that all the turbulators, the PEC was more than 1. The highest PEC was 1.91 for  $H = 0.71$ , and the lowest PEC was 1.08 for  $W = 0.71$ , as shown in Fig. 21. The results demonstrated that the change in the width of the ribs produced the lowest PEC. The change in rib width decreased the PEC of DTHE compared to using nanofluids without turbulator insertion. This decrease is attributed to the increase in the friction factor, which outweighs the increase in the Nusselt number.

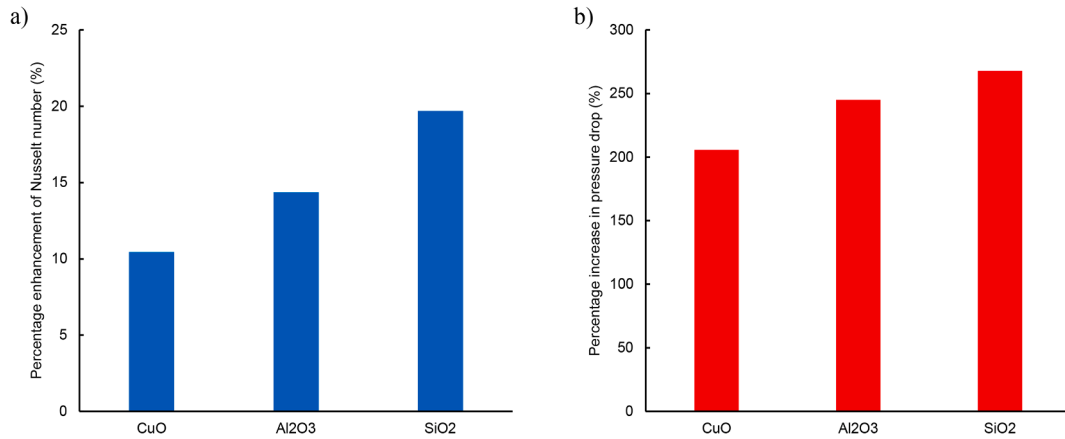


Fig. 17. Percentage enhancement of a) the average Nusselt number and b) pressure drop of the three nanofluids without turbulator insertion and with  $Re = 2000$  and a volume fraction  $\phi = 0.05$ , compared to water and without turbulator insertion.

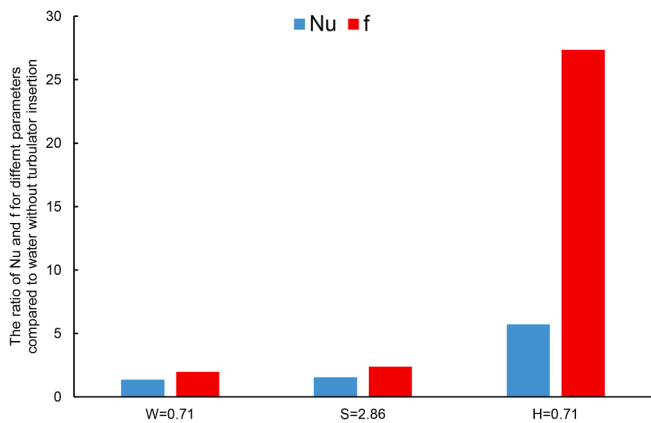


Fig. 18. The ratio of average Nusselt number and friction factor for SiO<sub>2</sub> and various dimensionless parameters, W, S, and H, to the average Nusselt number and friction factor of water without turbulator insertion.

### 6. Conclusions

In this numerical research, a single-phase model of different nanofluids was employed to investigate the effects of different shapes and geometrical parameters of turbulator insertion on the laminar heat transfer and fluid flow characteristics in a DTHE with counter flow configuration. The hydrothermal characteristics of four different shapes, including triangular, rectangular, trapezoidal and oval, with changing the width, height and distances between the ribs were presented. The results were compared to the case without turbulator insertion in pure water. The key findings of the research are outlined below.

- The trapezoidal and triangular ribs respectively showed the highest average Nusselt number and friction factor compared to other ribs.
- The change in the height of the ribs had the most impact on the average Nusselt number and friction factor compared to the change in width and distance between the ribs.
- The SiO<sub>2</sub> nanofluid showed a better heat transfer rate enhancement than Al<sub>2</sub>O<sub>3</sub> and CuO.
- The maximum PEC achieved was 1.2 and 1.9 respectively for the nanofluid without turbulator insertion and nanofluid with turbulator insertion.
- The trapezoidal ribs had the highest heat transfer, but the oval shape had a better PEC because it had a lower friction factor.

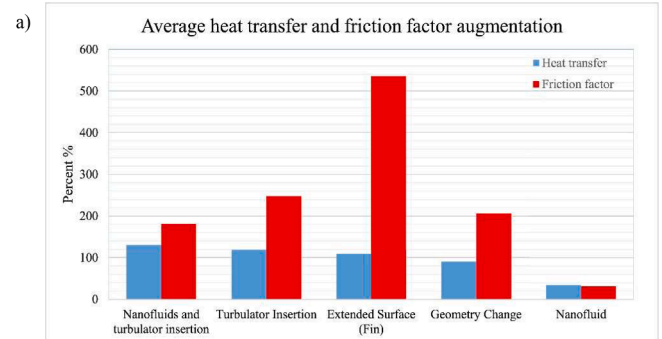
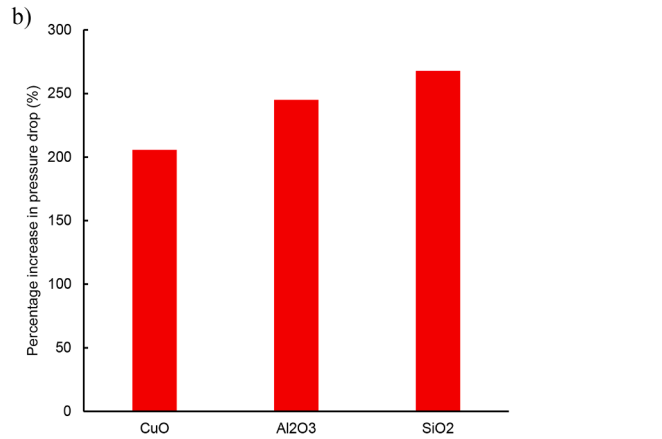


Fig. 19. Statistical investigation presented by Tavousi, et al. (E. Tavousi, N. Perera, D. Flynn, and R. Hasan, "Heat transfer and fluid flow characteristics of the passive method in double tube heat exchangers: a critical review," International Journal of Thermofluids, p., 2023) a) increase in heat transfer and friction factor and b) increase in heat transfer of different techniques (box and whisker plot).

### CRediT authorship contribution statement

**Ebrahim Tavousi:** Writing – original draft, Validation, Software, Methodology, Investigation, Formal analysis. **Noel Perera:** Writing – review & editing, Supervision, Resources, Project administration, Methodology, Conceptualization. **Dominic Flynn:** Writing – review & editing, Supervision. **Reaz Hasan:** Supervision, Project administration, Formal analysis. **Mostafizur Rahman:** Writing – review & editing, Supervision, Methodology.

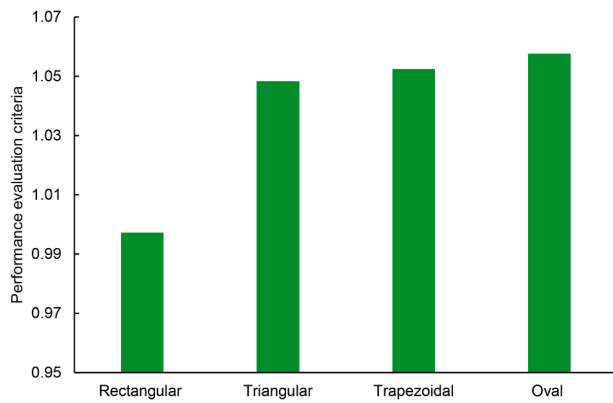


Fig. 20. PEC for the different shapes of ribs.

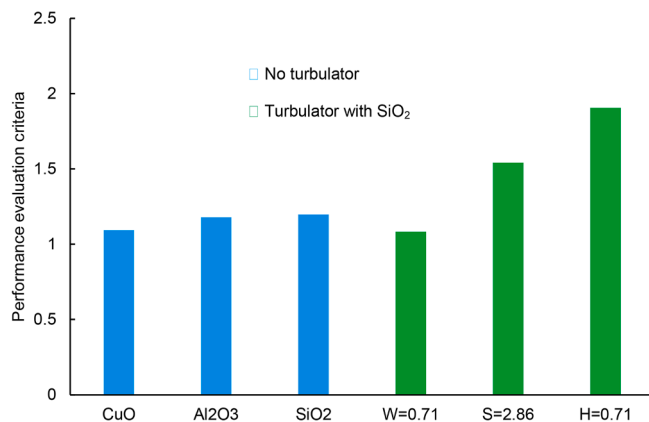


Fig. 21. The maximum PEC achieved for all cases.

## Declaration of competing interest

The authors declare that they have no known competing financial interests or personal relationships that could have appeared to influence the work reported in this paper.

## Data availability

Data will be made available on request.

## Acknowledgement

The authors thank Dr Roger Tait for his advice and guidance on the use of the High Performance Computing (Cluster 3) resource. The authors also thank the Faculty of Computing, Engineering and the Built Environment at Birmingham City University for supporting this High Performance Computing resource.

## References

- Ahmed, H.E., Ahmed, M., Seder, I.M., Salman, B., 2016. Experimental investigation for sequential triangular double-layered microchannel heat sink with nanofluids. *Int. Commun. Heat Mass Transfer* 77, 104–115.
- Akbari, O.A., Toghraie, D., Karimipour, A., Marzban, A., Ahmadi, G.R., 2017. The effect of velocity and dimension of solid nanoparticles on heat transfer in non-Newtonian nanofluid. *Physica E* 86, 68–75.
- Alam, T., Kim, M.-H., 2018. A comprehensive review on single phase heat transfer enhancement techniques in heat exchanger applications. *Renew. Sustain. Energy Rev.* 81, 813–839.
- Albojajmal, A., Vafai, K., 2017. Analysis of single phase, discrete and mixture models, in predicting nanofluid transport. *Int. J. Heat Mass Transf.* 114, 225–237.
- Bergman, T., 2009. Effect of reduced specific heats of nanofluids on single phase, laminar internal forced convection. *Int. J. Heat Mass Transf.* 52 (5–6), 1240–1244.

- E. Tavousi, N. Perera, D. Flynn, and R. Hasan, “Heat transfer and fluid flow characteristics of the passive method in double tube heat exchangers: a critical review,” *International Journal of Thermofluids*, p. 100282, 2023, doi: 10.1016/j.ijft.2023.100282.
- E. Tavousi, N. Perera, D. Flynn, and R. Hasan, “Numerical Investigation of Heat Transfer and Fluid Flow Characteristics of Al<sub>2</sub>O<sub>3</sub> Nanofluid In A Double Tube Heat Exchanger With Turbulator Insertion,” *Proceedings of the 9th World Congress on Mechanical, Chemical, and Material Engineering (MCM'23)*, August 06-08 2023, doi: 10.11159/hdff23.218.
- E. Tavousi, N. Perera, D. Flynn, and R. Hasan, “Numerical investigation of laminar heat transfer and fluid flow characteristics of Al<sub>2</sub>O<sub>3</sub> nanofluid in a double tube heat exchanger,” *International Journal of Numerical Methods for Heat & Fluid Flow*, 2023, doi: 10.1108/HFF-03-2023-0114.
- Eiamsa-ard, S., Pethkool, S., Thianpong, C., Promvong, P., 2008. Turbulent flow heat transfer and pressure loss in a double pipe heat exchanger with louvered strip inserts. *Int. Commun. Heat Mass Transfer* 35 (2), 120–129.
- El Maakoul, A., Feddi, K., Saadeddine, S., Abdellah, A.B., El Metoui, M., 2020. Performance enhancement of finned annulus using surface interruptions in double-pipe heat exchangers. *Energ. Convers. Manage.* 210, 112710.
- Eshgarf, H., Nadooshan, A.A., Raisi, A., 2023. A review of multi-phase and single-phase models in the numerical simulation of nanofluid flow in heat exchangers. *Eng. Anal. Bound. Elem.* 146, 910–927.
- Gnanavel, C., Saravanan, R., Chandrasekaran, M., 2020. Heat transfer augmentation by nano-fluids and Spiral Spring insert in Double Tube Heat Exchanger—A numerical exploration. *Mater. Today: Proc.* 21, 857–861.
- Gnielinski, V., 1976. New equations for heat and mass transfer in turbulent pipe and channel flow. *Int. Chem. Eng.* 16 (2), 359–367.
- Hangi, M., Rahbari, A., Wang, X., Lipiński, W., 2022. Hydrothermal characteristics of fluid flow in a circular tube fitted with free rotating axial-turbine-type swirl generators: Design, swirl strength, and performance analyses. *Int. J. Therm. Sci.* 173, 107384.
- Hausen, H., 1959. Neue Gleichungen für die Wärmeübertragung bei freier oder erzwungener Strömung. *Allg. Waermetech* 9, 75–79.
- Heyhat, M., Kowsary, F., Rashidi, A., Momenpour, M., Amrollahi, A., 2013. Experimental investigation of laminar convective heat transfer and pressure drop of water-based Al<sub>2</sub>O<sub>3</sub> nanofluids in fully developed flow regime. *Exp. Therm Fluid Sci.* 44, 483–489.
- Hosseinzadeh, K., Moghaddam, M.E., Asadi, A., Mogharrebi, A., Ganji, D., 2020. Effect of internal fins along with hybrid nano-particles on solid process in star shape triplex latent heat thermal energy storage system by numerical simulation. *Renew. Energy* 154, 497–507.
- Hussain, M., Sheremet, M., 2023. Convection analysis of the radiative nanofluid flow through porous media over a stretching surface with inclined magnetic field. *Int. Commun. Heat Mass Transfer* 140, 106559.
- Incropera, F.P., DeWitt, D.P., Bergman, T.L., Lavine, A.S., 1996. *Fundamentals of heat and mass transfer*. Wiley, New York.
- Iwaniszyn, M., et al., 2021. Entrance effects on forced convective heat transfer in laminar flow through short hexagonal channels: Experimental and CFD study. *Chem. Eng. J.* 405, 126635.
- Jadhav, M., Awari, R., Bibe, D., Bramhane, A., Mokashi, M., 2016. Review on enhancement of heat transfer by active method. *International Journal of Current Engineering and Technology* 6, 221–225.
- Kamyar, A., Saidur, R., Hasanuzzaman, M., 2012. Application of computational fluid dynamics (CFD) for nanofluids. *Int. J. Heat Mass Transf.* 55 (15–16), 4104–4115.
- Karupphasamy, M., Saravanan, R., Chandrasekaran, M., Muthuraman, V., 2020. Numerical exploration of heat transfer in a heat exchanger tube with cone shape inserts and Al<sub>2</sub>O<sub>3</sub> and CuO nanofluids. *Mater. Today: Proc.* 21, 940–947.
- Kumar, N.R., Bharamara, P., Sundar, L.S., Singh, M.K., Sousa, A.C., 2017. Heat transfer, friction factor and effectiveness of Fe<sub>3</sub>O<sub>4</sub> nanofluid flow in an inner tube of double pipe U-bend heat exchanger with and without longitudinal strip inserts. *Exp. Therm Fluid Sci.* 85, 331–343.
- Lakew, A.A., Bolland, O., 2010. Working fluids for low-temperature heat source. *Appl. Therm. Eng.* 30 (10), 1262–1268.
- Lalegani, F., Saffarian, M.R., Moradi, A., Tavousi, E., 2018. Effects of different roughness elements on friction and pressure drop of laminar flow in microchannels. *Int. J. Numer. Meth. Heat Fluid Flow* 28 (7), 1664–1683. <https://doi.org/10.1108/HFF-04-2017-0140>.
- Li, H., et al., 2022. A comprehensive review of heat transfer enhancement and flow characteristics in the concentric pipe heat exchanger. *Powder Technol.* 397, 117037.
- Lin, J., Hong, Y., Lu, J., 2022. New method for the determination of convective heat transfer coefficient in fully-developed laminar pipe flow. *Acta Mech. Sin.* 38 (1), 1–10.
- Liu, S., Sakr, M., 2013. A comprehensive review on passive heat transfer enhancements in pipe exchangers. *Renew. Sustain. Energy Rev.* 19, 64–81.
- Louis, S.P., Ushak, S., Milian, Y., Nems, M., Nems, A., 2022. Application of Nanofluids in Improving the Performance of Double-Pipe Heat Exchangers—A Critical Review. *Materials* 15 (19), 6879.
- Luo, C., Song, K., 2021. Thermal performance enhancement of a double-tube heat exchanger with novel twisted annulus formed by counter-twisted oval tubes. *Int. J. Therm. Sci.* 164, 106892.
- Maleki, N.M., Pourahmad, S., Khoshkhoo, R.H., Ameri, M., 2023. Performance improvement of a double tube heat exchanger using novel electromagnetic vibration (EMV) method in the presence of Al<sub>2</sub>O<sub>3</sub>-water and CuO-water nanofluid; An experimental study. *Energy* 281, 128193.

- Mohammed, H., Hasan, H.A., Wahid, M., 2013. Heat transfer enhancement of nanofluids in a double pipe heat exchanger with louvered strip inserts. *Int. Commun. Heat Mass Transfer* 40, 36–46.
- Noorbakhsh, M., Ajarostaghi, S.S.M., Zabolli, M., Kiani, B., 2022. Thermal analysis of nanofluids flow in a double pipe heat exchanger with twisted tapes insert in both sides. *J. Therm. Anal. Calorim.* 147 (5), 3965–3976.
- Omidi, M., Farhadi, M., Jafari, M., 2017. A comprehensive review on double pipe heat exchangers. *Appl. Therm. Eng.* 110, 1075–1090.
- Padmanabhan, S., Reddy, O.Y., Yadav, K.V.A.K., Raja, V.B., Palanikumar, K., 2021. Heat transfer analysis of double tube heat exchanger with helical inserts. *Mater. Today: Proc.* 46, 3588–3595.
- Pourahmad, S., Pestei, S., 2016. Effectiveness-NTU analyses in a double tube heat exchanger equipped with wavy strip considering various angles. *Energ. Convers. Manage.* 123, 462–469.
- Prasad, P.D., Gupta, A., 2016. Experimental investigation on enhancement of heat transfer using Al<sub>2</sub>O<sub>3</sub>/water nanofluid in a u-tube with twisted tape inserts. *Int. Commun. Heat Mass Transfer* 75, 154–161.
- Rao, V.N., Sankar, B.R., 2019. Heat transfer and friction factor investigations of CuO nanofluid flow in a double pipe U-bend heat exchanger. *Mater. Today: Proc.* 18, 207–218.
- W. M. Rohsenow, J. P. Hartnett, and Y. I. Cho, *Handbook of heat transfer*. McGraw-Hill New York, 1998.
- Shah, R.K., London, A.L., 2014. *Laminar flow forced convection in ducts: a source book for compact heat exchanger analytical data*. Academic press.
- Sharma, K., Sarma, P., Azmi, W., Mamat, R., Kadirgama, K., 2012. Correlations to predict friction and forced convection heat transfer coefficients of water based nanofluids for turbulent flow in a tube. *International Journal of Microscale and Nanoscale Thermal and Fluid Transport Phenomena* 3 (4), 1–25.
- Shirvan, K.M., Mamourian, M., Mirzakhani, S., Ellahi, R., 2017. Numerical investigation of heat exchanger effectiveness in a double pipe heat exchanger filled with nanofluid: a sensitivity analysis by response surface methodology. *Powder Technol.* 313, 99–111.
- Sieder, E.N., Tate, G.E., 1936. Heat transfer and pressure drop of liquids in tubes. *Ind. Eng. Chem.* 28 (12), 1429–1435.
- Singh, S.K., Sarkar, J., 2020. Improving hydrothermal performance of hybrid nanofluid in double tube heat exchanger using tapered wire coil turbulator. *Adv. Powder Technol.* 31 (5), 2092–2100.
- Singh, S.K., Sarkar, J., 2021. Thermohydraulic behavior of concentric tube heat exchanger inserted with conical wire coil using mono/hybrid nanofluids. *Int. Commun. Heat Mass Transfer* 122, 105134.
- Tian, L.-L., Liu, X., Chen, S., Shen, Z.-G., 2020. Effect of fin material on PCM melting in a rectangular enclosure. *Appl. Therm. Eng.* 167, 114764.
- Vajjha, R.S., Das, D.K., 2009. Experimental determination of thermal conductivity of three nanofluids and development of new correlations. *Int. J. Heat Mass Transf.* 52 (21–22), 4675–4682.
- Venkatesh, B., et al., 2023. Design Optimization of Counter-Flow Double-Pipe Heat Exchanger Using Hybrid Optimization Algorithm. *Processes* 11 (6), 1674.
- White, F.M., 1979. *Fluid mechanics*. Tata McGraw-Hill Education.
- Z. Cancan, L. Yafei, W. Li, X. Ke, and W. Jinxing, “Review heat exchanger: Research development of self-rotating inserts in heat exchanger tubes,” 2014.